Supporting Information

for

Binding and Exchange Reactions of Hydrogen Isotopes on Surfaces of Dispersed Pt Nanoparticles

Samuel L. Leung[1]
David Hibbitts[2]
Monica Garcia-Dieguez[1,3]
Enrique Iglesia[1*]

[1]Department of Chemical Engineering
University of California at Berkeley
Berkeley, CA 94720, U.S.A.

[2]Department of Chemical Engineering
University of Florida
Gainesville, FL, 32611, U.S.A.

[3]Current address: Johnson Matthey
Billingham, TS23 1LB, United Kingdom

* To whom correspondence should be addressed
E-mail: iglesia@cchem.berkeley.edu
Tel: (510) 642-9673
Fax: (510) 642-4778

SI-1 Effect of Catalyst Pellet Size on Reaction Rates

H_2-D_2 isotopic exchange kinetics were obtained on 0.2% Pt/SiO_2-A catalyst powders sieved to retain particles smaller than 100 μm and on powders further ground to a fine powder (<50 μm). These rates were compared to confirm the absence of mass transport limitations on these catalytic samples. Figure S1 shows exchange rates (2 kPa H_2, 2 kPa D_2) as a function of temperature in an Arrhenius plot for these samples and the ratio of these rates (r_{small}/r_{large}; r_{small} =rates on ground fine powders <50 μm, r_{large}=rates on the sieved particles <100 μm) for temperatures between 600 and 1000 K, which represents the temperatures most likely to be mass-transport limited in this study. Rates were nearly identical for both samples, indicating the absence of such mass-transport artifacts.

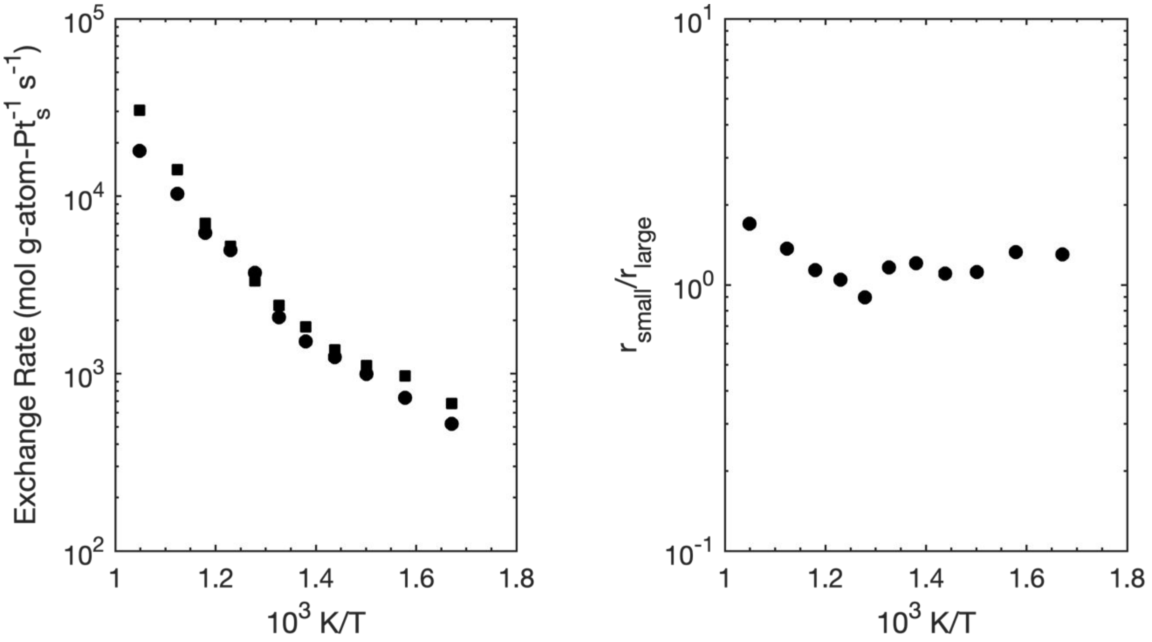

Figure S1. (a) Arrhenius plot of H_2-D_2 isotopic exchange rates (2 kPa H_2, 2 kPa D_2) on 0.2% Pt/SiO_2-A powders <100 μm (●) and <50 μm (■) (2 kPa H_2, 2 kPa D_2; 0.167 K s^{-1} heating rate). (b) Ratio of exchange rates obtained on fine, ground powders (<50 μm) to those on sieved powders (<100 μm).

SI-2 H_2 and D_2 Chemisorption Isotherms on Pt/γ-Al_2O_3-B at 523-673 K

H_2 and D_2 adsorption isotherms were obtained for a range of temperatures (523-673 K) on 1.6% wt. Pt/γ-Al_2O_3-B (Fig. S2). These isotherms were used to extract the equilibrium constants for H_2 (K_H) and D_2 (K_D) adsorption (Fig. S3) as a function of temperature (at various fractional coverages of the Pt surface). The ratios of K_H/K_D (TIE) were only weakly dependent on fractional surface coverages and were thus averaged across these coverages for a given temperature (Fig. S3); these ratios are shown in Figure 3 in the main text.

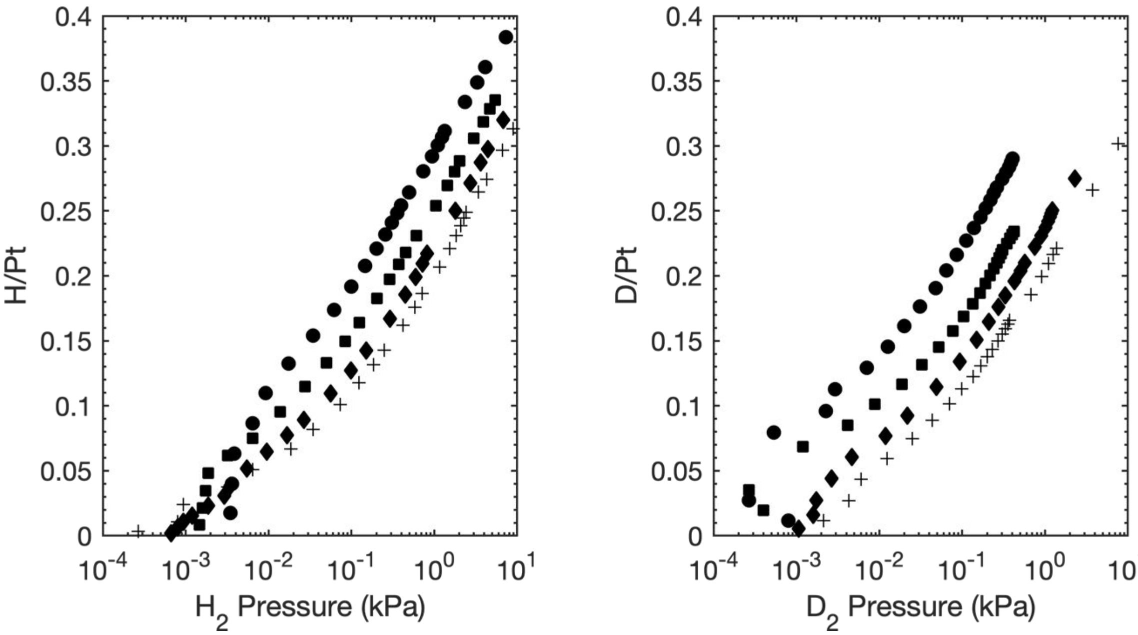

Figure S2. (a) H_2 and (b) D_2 dissociative adsorption isotherms on Pt/γ-Al_2O_3-B at (●) 523, (■) 573, (◆) 623, and (+) 673 K.

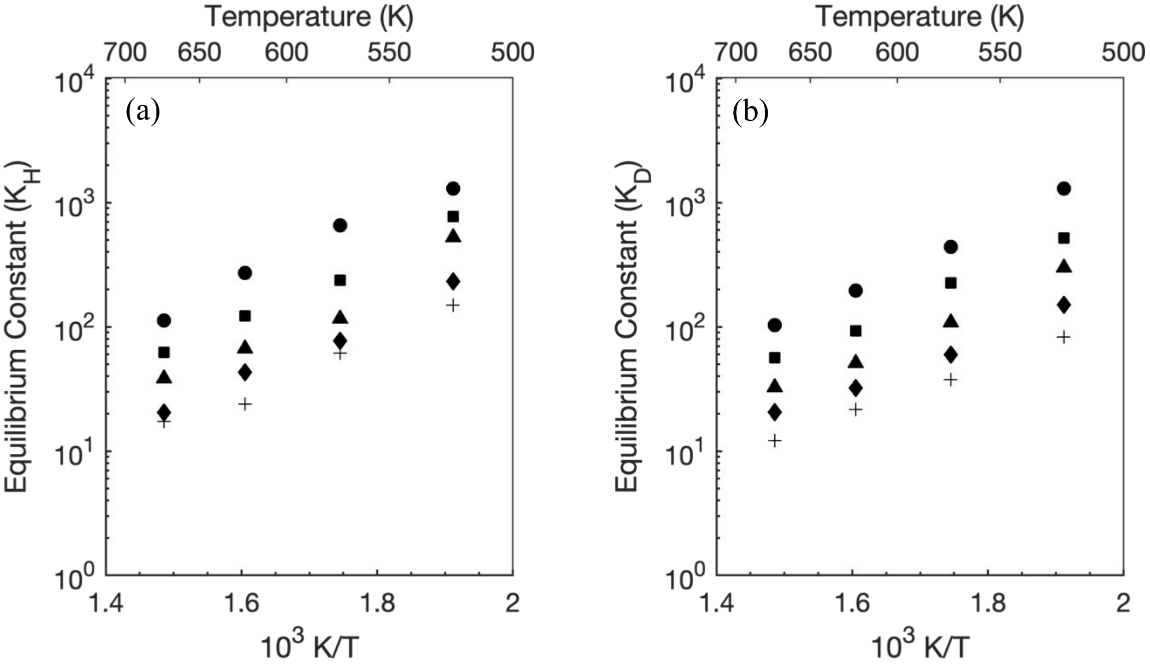

Figure S3. Equilibrium constants vs. temperature for the adsorption of (a) H_2 (K_H) and (b) D_2 (K_D) on Pt/γ-Al_2O_3-B at fractional surface coverages of 0.19 (●), 0.28 (■), 0.38 (▲), 0.47 (◆), and 0.57 (+).

SI-3 Derivation of Rate Equations for H_2-D_2 Exchange Mechanisms

SI-3.1 Derivation of Expressions for H* and D* Surface Coverages and the Rate Equation for HD Formation from the Reaction Between H* and D* Adatoms

$$H_2 + 2^* \underset{k_{-1}}{\overset{k_1}{\rightleftarrows}} 2H^* \qquad [S1.1]$$

$$HD + 2^* \xleftarrow[k_{-2}]{} H^* + D^* \qquad [S1.2]$$

$$D_2 + 2^* \underset{k_{-3}}{\overset{k_3}{\rightleftarrows}} 2D^* \qquad [S1.3]$$

Scheme S1. Elementary steps for H_2 and D_2 dissociation and recombination

Scheme S1 shows the conventional representation of H_2-D_2 dissociation, recombination, and exchange. The rate of HD formation ($r_{HD,f}$) is given by:

$$r_{HD,f} = k_{-2}\theta_H\theta_D \qquad (SI-1)$$

Here, θ_H and θ_D are the fractional coverages of the metal surface by H* and D* adatoms, respectively. These fractional coverages can be found by applying the pseudo-steady-state approximation (PSSA) to H*:

$$2r_{1.1} = 2r_{-1.1} + r_{-1.2} \qquad (SI-2)$$

$$2k_1(H_2)\theta_s^2 = k_{-1}\theta_H^2 + k_{-2}\theta_H\theta_D \qquad (SI-3)$$

and D*:

$$2r_{1.3} = r_{-1.2} + 2r_{-1.3} \qquad (SI-4)$$

$$2k_1(D_2)\theta_s^2 = k_{-2}\theta_H\theta_D + k_{-3}\theta_D^2 \qquad (SI-5)$$

Here, $r_{1.i}$ and $r_{-1.i}$ are the forward and reverse rates of reaction i in Scheme S1. We note that $r_{-1.1}$ and $r_{-1.3}$ are divided by 2 to avoid double-counting H*-H* and D*-D* reactions. H_2 and D_2 adsorption was shown to exhibit a mild TIE (denoted here as $TIE_{D2} = K_1/K_3$) in Section 3.2. For the dissociative adsorption of HD, the TIE was assumed to be halved, such that:

$$TIE_{HD} = \frac{TIE_{D2} + 1}{2} \qquad (SI - 6)$$

The equilibrium constants for H_2, HD, and D_2 adsorption are related to the rate constants for steps 1.1-1.3 in Scheme S1 by:

$$K_i = \frac{k_i}{k_{-i}} \qquad (SI - 7)$$

The TIE must therefore be reflected in the rate constants as a KIE:

$$K_1 \equiv \frac{k_1}{k_{-1}} = TIE_{HD} K_2 \equiv TIE_{HD} \frac{k_2}{k_{-2}} = TIE_{D2} K_3 \equiv TIE_{D2} \frac{k_3}{k_{-3}} \qquad (SI - 8)$$

Next, we assumed that the rate constant for adsorption is equal for H_2, HD, and D_2 $(k_1 = k_2 = k_3)$. The relation between desorption rate constants is therefore given by:

$$k_{-1} = \frac{k_{-2}}{TIE_{HD}} = \frac{k_{-3}}{TIE_{D2}} \qquad (SI - 9)$$

These equations (Eq. SI-2 – SI-9), along with the assumption that the surface is covered,

$$\theta_H + \theta_D = 1 \qquad (SI - 10)$$

can be solved to give the following expressions for H* and D* coverage:

$$\theta_H = \frac{(D_2) - (H_2) + (D_2)TIE_{D2} + 3(H_2)TIE_{D2} - \beta}{2((H_2) + (D_2))(TIE_{D2} - 1)} \qquad (SI - 11)$$

$$\theta_D = \frac{-3(D_2) - (H_2) + (D_2)TIE_{D2} - (H_2)TIE_{D2} + \beta}{2((H_2) + (D_2))(TIE_{D2} - 1)} \qquad (SI - 12)$$

$$\beta = \sqrt{8(D_2)((H_2) + (D_2))(TIE_{D2} - 1) + (3(D_2) + (H_2) - (D_2)TIE_{D2} + (H_2)TIE_{D2})^2} \qquad (SI - 13)$$

In the absence of a TIE (TIE_{D2} = 1), Equations SI-2 – SI-5 and SI-10 can be solved to give:

$$\theta_H = \frac{(H_2)}{(H_2) + (D_2)} \qquad (SI - 14)$$

$$\theta_D = \frac{(D_2)}{(H_2) + (D_2)} \qquad (SI - 15)$$

and the equation for the formation rate of HD (Eq. SI-1) can be written as:

$$r_{HD,f} = k_{-1} \frac{(H_2)(D_2)}{((H_2) + (D_2))^2} \qquad (SI - 16)$$

SI-3.2 Derivation of Rate Equation for HD Formation from the Reaction Between H_2 and D_2 with H*-H*, H*-D*, and D*-D* Pairs

The reaction between H_2 and D_2 with H*-H*, H*-D*, and D*-D* site pairs is considered here, as represented by the diagram and elementary steps in Scheme S2.

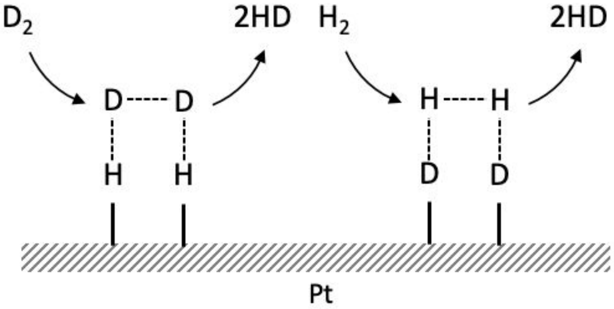

$$2\,H_2 + 2* \underset{k_{-3}}{\overset{k_3}{\rightleftarrows}} H_2 + 2H* \qquad [S2.1]$$

$$H_2 + HD + 2* \underset{k_{-3}}{\overset{k_3}{\rightleftarrows}} H_2 + H* + D* \qquad [S2.2]$$

$$H_2 + HD + 2* \underset{k_{-3}}{\overset{k_3}{\rightleftarrows}} HD + 2H* \qquad [S2.3]$$

$$HD + HD + 2* \underset{k_{-3}}{\overset{k_3}{\rightleftarrows}} H_2 + 2D* \qquad [S2.4]$$

$$HD + HD + 2* \underset{k_{-3}}{\overset{k_3}{\rightleftarrows}} HD + H* + D* \qquad [S2.5]$$

$$HD + HD + 2* \underset{k_{-3}}{\overset{k_3}{\rightleftarrows}} D_2 + 2H* \qquad [S2.6]$$

$$HD + D_2 + 2* \underset{k_{-3}}{\overset{k_3}{\rightleftarrows}} D_2 + H* + D* \qquad [S2.7]$$

$$HD + D_2 + 2* \underset{k_{-3}}{\overset{k_3}{\rightleftarrows}} HD + 2D* \qquad [S2.8]$$

$$2\,D_2 + 2* \underset{k_{-3}}{\overset{k_3}{\rightleftarrows}} D_2 + 2D* \qquad [S2.9]$$

Scheme S2. Elementary steps for H_2-D_2 isotopic exchange via the adsorption-assisted desorption of H*-H* and D*-D* site pairs.

Scheme S2 assumes negligible KIEs for all reactions. The forward rate for HD formation ($r_{HD,f}$) from the elementary steps in Scheme S2 is given by:

$$r_{HD,f} = 2k_{-3}(H_2)\theta_D^2 + k_{-3}(H_2)\theta_H\theta_D + k_{-3}(D_2)\theta_H\theta_D + 2k_{-3}(D_2)\theta_H^2 \qquad (SI-17)$$

Here, θ_H and θ_D are the fractional coverage of the metal surface by H and D adatoms, respectively. Applying the pseudo-steady-state approximations (PSSA) on H* and D* and assuming that the reaction is far from equilibrium (the pressure of HD is small) gives the following expression for H*:

$$2r_{2.1} = 2r_{-2.1} + r_{-2.2} + 2r_{-2.6} + r_{-2.7} \qquad (SI-18)$$

$$2k_3(H_2)^2\theta_s^2 = 2k_{-3}(H_2)\theta_H^2 + k_{-3}(H_2)\theta_H\theta_D + 2k_{-3}(D_2)\theta_H^2 + k_{-3}(D_2)\theta_H\theta_D \qquad (SI-19)$$

and D*:

$$2r_{2.9} = r_{-2.2} + 2r_{-2.4} + r_{-2.7} + 2r_{-2.9} \qquad (SI-20)$$

$$2k_3(D_2)^2\theta_s^2 = k_{-3}(H_2)\theta_H\theta_D + 2k_{-3}(H_2)\theta_D^2 + k_{-3}(D_2)\theta_H\theta_D + 2k_{-3}(D_2)\theta_D^2 \qquad (SI-21)$$

$r_{2.i}$ and $r_{-2.i}$ are the forward and reverse rates of reaction i in Scheme S2. By assuming that the surface is covered by H* and D*, such that

$$\theta_H + \theta_D = 1 \qquad (SI-22)$$

expressions for θ_H and θ_D can be obtained:

$$\theta_H = -\frac{4(H_2)^2}{(D_2)^2 + 3(H_2)^2 - \gamma} \qquad (SI-23)$$

$$\theta_D = -\frac{4(D_2)^2}{(H_2)^2 + 3(D_2)^2 - \gamma} \qquad (SI-24)$$

$$\gamma = \sqrt{(H_2)^4 + 14(H_2)^2(D_2)^2 + (D_2)^4} \qquad (SI-25)$$

Equation SI-17 can therefore be written as:

$$\begin{aligned} r_{HD,f} = {} & [64\,k_{-3}(H_2)(D_2)((H_2) + (D_2)) \\ & \{(H_2)^6 + (D_2)^6 + 11(H_2)^2(D_2)^4 + 11(D_2)^2(H_2)^4 - \gamma((H_2)^4 + (D_2)^4 + 4(H_2)^2(D_2)^2)\}] \\ & \div \left[\left(3(H_2)^2 + (D_2)^2 - \gamma\right)^2\left(3(D_2)^2 + (H_2)^2 - \gamma\right)^2\right] \end{aligned} \qquad (SI-26)$$

This equation, as in the case of HD formation solely from the recombinative desorption of H* and D* (Section S3.1) predicts a maximum in the rate at equimolar H_2 and D_2 feeds and thus contradicts the kinetic evidence in this study.

SI-3.3 Derivation of Rate Equation for HD Formation from H*-D*, H_2-D*, and D_2-H* Reactions

$$H_2 + 2^* \underset{k_{-1}}{\overset{k_1}{\rightleftharpoons}} 2H^* \qquad [S3.1]$$

$$HD + 2^* \xleftarrow[k_{-2}]{} H^* + D^* \qquad [S3.2]$$

$$D_2 + 2^* \underset{k_{-3}}{\overset{k_3}{\rightleftharpoons}} 2D^* \qquad [S3.3]$$

$$H_2 + D^* \xrightarrow{k_4} HD + H^* \qquad [S3.4]$$

$$D_2 + H^* \xrightarrow{k_5} HD + D^* \qquad [S3.5]$$

Scheme S3. Elementary steps for H_2-D_2 isotopic exchange via the reaction between H_2 and D_2 with D* and H* adatoms.[*]

The rate for HD formation ($r_{HD,f}$) from the elementary steps in Scheme S3 is given by:

$$r_{HD,f} = k_{-2}\theta_H\theta_D + k_4(H_2)\theta_D + k_5(D_2)\theta_H \qquad (SI-27)$$

Here, θ_H and θ_D are the fractional coverage of the metal surface by H and D adatoms, respectively. We apply the pseudo-steady-state approximation (PSSA) to H*

$$2r_{3.1} + r_{3.4} = r_{-3.1} + r_{-3.2} + r_{3.5} \qquad (SI-28)$$

$$2k_1(H_2)\theta_s^2 + k_4(H_2)\theta_D = k_{-1}\theta_H^2 + k_{-2}\theta_H\theta_D + k_5(D_2)\theta_H \qquad (SI-29)$$

and D*

$$2r_{3.3} + r_{3.5} = r_{-3.2} + r_{-3.3} + r_{3.4} \qquad (SI-30)$$

$$2k_1(D_2)\theta_s^2 + k_5(D_2)\theta_H = k_{-2}\theta_H\theta_D + k_{-3}\theta_D^2 + k_4(H_2)\theta_D \qquad (SI-31)$$

These equations assume that the reaction is far from equilibrium, such that (HD) is small. Exchange rates also increased monotonically with H_2 and D_2 pressures, even far above H_2/D_2 ratios

---

[*] This scheme is identical to Scheme 1 in the main text.

that represent equal coverages of H* and D*, indicating that the rates of dissociation and recombination ($r_{3.1}$, $r_{-3.1}$, $r_{3.2}$, $r_{-3.2}$, $r_{3.3}$, $r_{-3.3}$) are much slower than the reaction between H_2 and D* (or D_2 and H*) ($r_{3.4}$, $r_{3.5}$). These interpretations allow Equations SI-29 and SI-31 to be simplified to:

$$k_4(H_2)\theta_D = k_5(D_2)\theta_H \qquad (SI-32)$$

We define KIE_{ex} as:

$$KIE_{ex} = \frac{k_4}{k_5} \qquad (SI-33)$$

Equation SI-32 can therefore be written as:

$$k_4(H_2)\theta_D = \frac{k_4}{KIE_{ex}}(D_2)\theta_H \qquad (SI-34)$$

The surface is fully saturated during all H_2-D_2 exchange experiments, such that:

$$\theta_H + \theta_D = 1 \qquad (SI-35)$$

Equations SI-34 and SI-35 can be solved simultaneously to obtain expressions for θ_H and θ_D:

$$\theta_H = \frac{(H_2)KIE_{ex}}{(D_2) + (H_2)KIE_{ex}} \qquad (SI-36)$$

$$\theta_D = \frac{(D_2)}{(D_2) + (H_2)KIE_{ex}} \qquad (SI-37)$$

The rate of HD formation (Eq. SI-27) is therefore given by:

$$r_{HD,f} = \frac{k_{-2}KIE_{ex}(H_2)(D_2)}{((D_2) + (H_2)KIE_{ex})^2} + \frac{2k_4(H_2)(D_2)}{(D_2) + (H_2)KIE_{ex}} \qquad (SI-38)$$

HD formation rates were nearly identical when H_2 and D_2 pressures were interchanged, indicating that the rate constants k_4 and k_5 are equal ($KIE_{ex} = 1$; Eq. SI-33). Equation SI-38 can therefore be written as:

$$r_{HD,f} = k_{-2}\frac{(H_2)(D_2)}{((H_2) + (D_2))^2} + 2k_4\frac{(H_2)(D_2)}{(H_2) + (D_2)} \qquad (SI-39)$$

SI-4 Parity Plots of H_2-D_2 Exchange Models

Figure S4 shows parity plots of H_2-D_2 exchange rates on Pt/SiO_2-A for each of the H_2-D_2 exchange models considered, including the recombination of H* and D* (Scheme S1), the reaction between H_2 and D_2 with H*-H*, H*-D*, and D*-D* pairs (Scheme S2), and H_2-D* and D_2-H* reactions (Scheme S3).

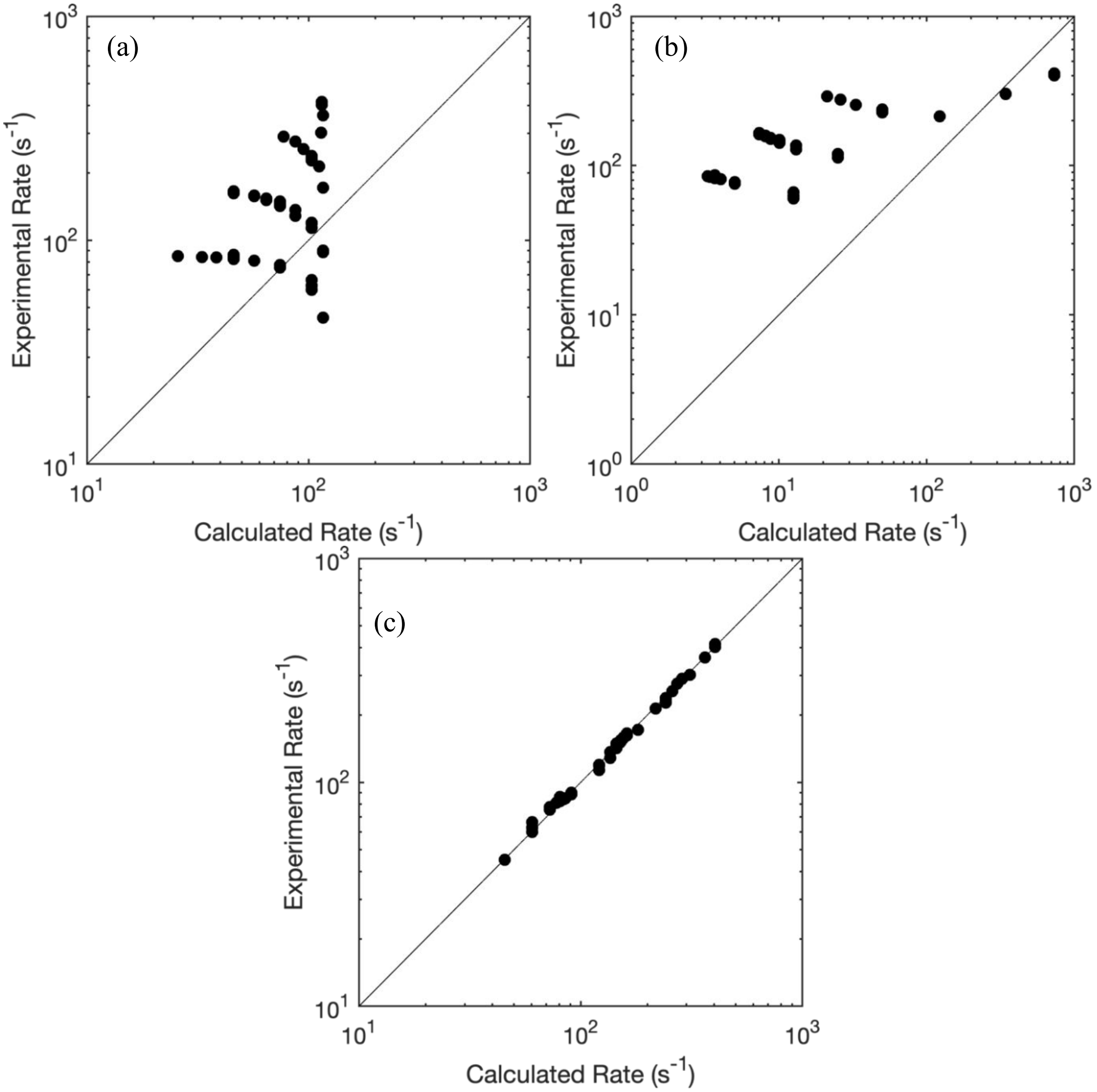

Figure S4. Parity plots of HD formation rates (a) H* and D* recombination reactions (Scheme S1) (b) H_2 and D_2 reactions with H*-H*, H*-D*, and D*-D* pairs (Scheme S2), and (c) H_2-D* and D_2-H* reactions (Scheme S3).

SI-5 Calculation of Exchange Rates Simulating Various Magnitudes of Kinetic Isotope Effects for H_2-D_2 Exchange

H_2-D_2 isotopic exchange rates were calculated using Eq. SI-38 for various KIE_{ex} values (Eq. SI-33; for H_2-D* and D_2-H* reactions; Steps 1.4 and 1.5, Scheme 1) to determine their effects on HD formation rates. We define $\gamma_{i,j}$ as the gas-phase composition with H_2 pressure i and D_2 pressure j, and $\chi_{i,j}$ as the ratio of rates:

$$\chi_{i,j} = \frac{r_{HD}(\gamma_{i,j})}{r_{HD}(\gamma_{j,i})} \qquad (SI-40)$$

Figure S5 shows this rate ratio $(\chi_{i,j})$ as a function of KIE_{ex} (Eq. SI-33) for several H_2/D_2 mixtures. These results show that $\chi_{i,j}$ depends only on the ratio of H_2 and D_2 pressures $\left(\frac{(H_2)}{(D_2)}\right)$ and not on the individual pressures. The simulated data also demonstrate that any difference in the values of these rate constants lead to clearly observable differences in the HD exchange rate when pressures are interchanged. The absence of such differences in the present work (Fig. 4-5) therefore reflects KIE_{ex} values near unity (1.1 ± 0.33).

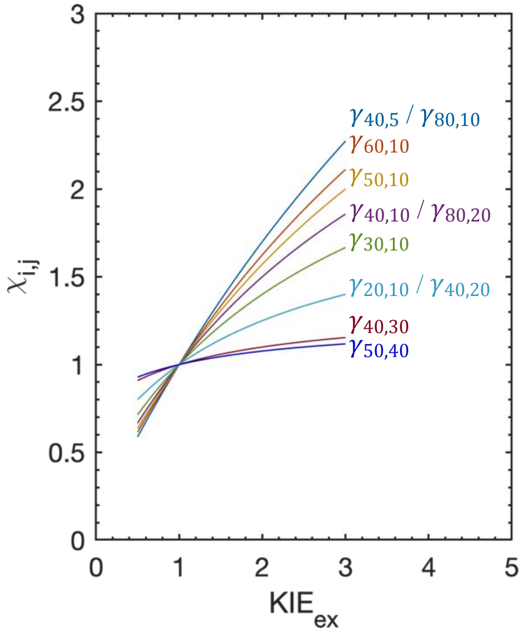

Figure S5. Calculated rate ratios $\left(\chi_{i,j} = \frac{r_{HD}(\gamma_{i,j})}{r_{HD}(\gamma_{j,i})}\right)$ as a function of a simulated kinetic isotope effect $\left(KIE_{ex} = \frac{k_4}{k_5}\right)$ for compositions of H_2 and D_2 $(\gamma_{i,j})$ where i is the H_2 pressure and j is the D_2 pressure.

SI-6 Sensitivity Analysis of Rate Parameters k_{-2} and k_4

The sensitivity of the proposed mechanistic model for H_2-D_2 exchange (Scheme 1) towards the values of k_{-2} and k_4 was investigated by calculating the sum of squared residuals (SSR) while k_4 was varied over factor of 1.5 from its regressed value (9.1 ± 0.2 kPa^{-1} s^{-1}) and k_{-2} was varied between 0.01 and 100. This range was chosen for k_{-2} to represent positive values that are physical in nature. The SSR values are plotted in a contour plot in Figure S5. The SSR increases from its minimum value of 0.047 to 1.124 (at a constant value of k_4, 9.1 kPa^{-1} s^{-1}) as k_{-2} increases, indicating that the exchange reaction is dominated by the reaction of H_2 with D* (or D_2 with H*). The SSR increases to a maximum value of 3.251 as k_4 is increased by a factor of 1.5 (at a constant value of k_{-2}, 0.01 kPa^{-1} s^{-1}). These results show the SSR is insensitive to the value of k_{-2} until much larger values (>10 kPa^{-1} s^{-1}) and reflect the difficulty in measuring H*+D* recombination rates, as shown also by the large uncertainty in the regressed value (-2.1 ± 20 s^{-1}).

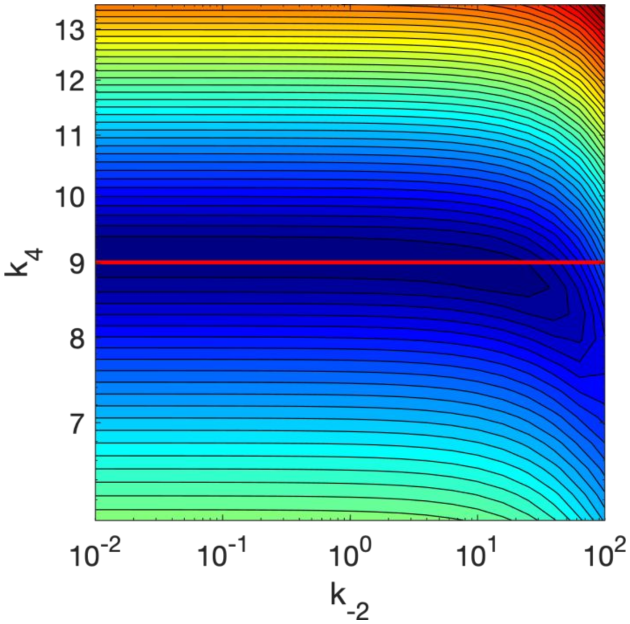

Figure S6. Contour plot of sum of squared residuals as k_4 is varied over factor of 1.5 from its regressed value (9.1 ± 0.2 kPa^{-1} s^{-1}, represented by red line) and k_{-2} is varied between 0.01 and 100.

SI-7 DFT-derived Hydrogen Adsorption Enthalpies as a Function of Coverage on Pt(111) Surfaces and Pt_{201} Particles

Adsorption enthalpies ($\Delta H_{H_2,ads}$) and differential adsorption enthalpies ($\delta H_{H_2,ads}$), given respectively by:

$$\Delta H_{H*,ads} = \frac{E[n\mathrm{H}^*] - 0.5n \cdot E[\mathrm{H}_2] - E[\mathrm{M}]}{n} \qquad (SI-41)$$

$$\delta H_{H*,ads} = \frac{E[(n+x)\mathrm{H}^*] - 0.5x \cdot E[\mathrm{H}_2] - E[n\mathrm{H}^*]}{x} \qquad (SI-42)$$

were calculated for a range of H*/Pt_s ratios on Pt(111) surfaces and Pt_{201} particles with H* bound predominantly at either atop or fcc sites, as shown in Figure S7. Here, n represents the number of H atoms, and x represents the number of added H atoms. The differential adsorption enthalpies from these data indicate that Pt(111) saturates at a H*/Pt_s ratio of 1, while Pt_{201} particles saturate at a H*/Pt_s ratio of 1.4. Structural images of the H*-covered clusters featuring predominantly atop or fcc H* adatoms (at H*/Pt_s ratios of 0.4-1.9) are shown in Figures S8 and S9, respectively.

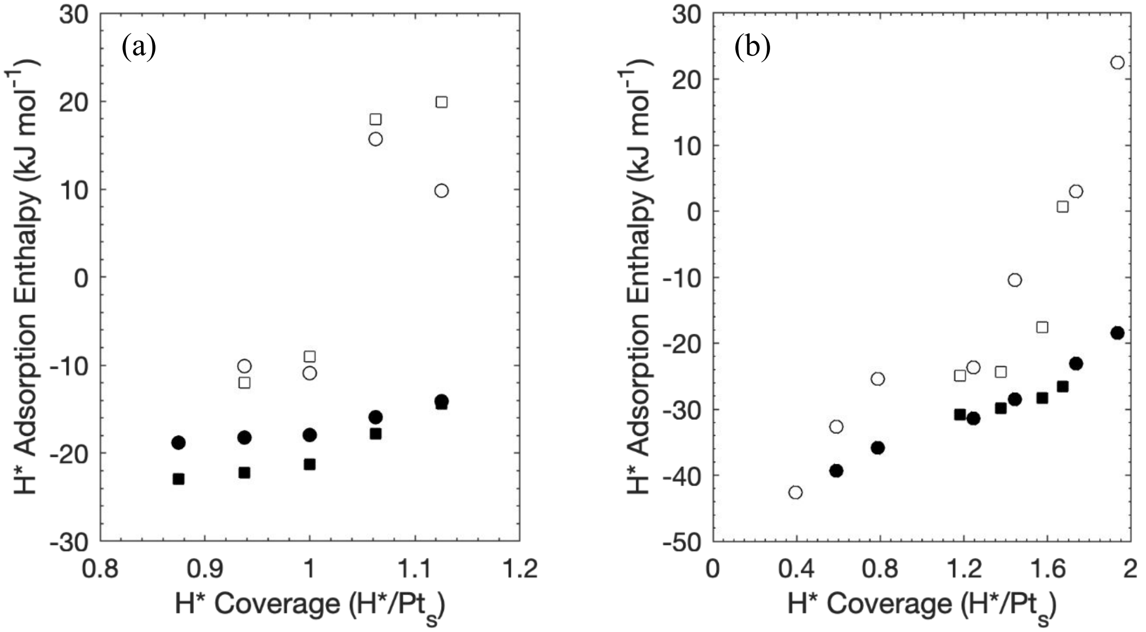

Figure S7. Adsorption enthalpies (relative to H_2(g), 383 K) for H* on (a) Pt(111) surfaces and (b) Pt_{201} particles. Filled symbols represent adsorption enthalpies averaged across all H*-adatoms (corresponding to ½ n H_2(g) + n* → nH*; $\Delta H_{H*,ads}$, Eq. SI-40) referenced to a bare Pt surface while hollow symbols denote differential binding enthalpies (corresponding to ½ x H_2(g) + nH* + x* → (n+x)H*; $\delta H_{H*,ads}$, Eq. SI-41), representing the average binding enthalpy of H* added between states. H* adatoms can present in either (●,○) atop or (■,□) fcc positions on Pt(111). H* adatoms are also present in predominantly (●,○) atop or (■,□) fcc binding modes on Pt_{201}, but H* occupies a mixture of sites in both cases.

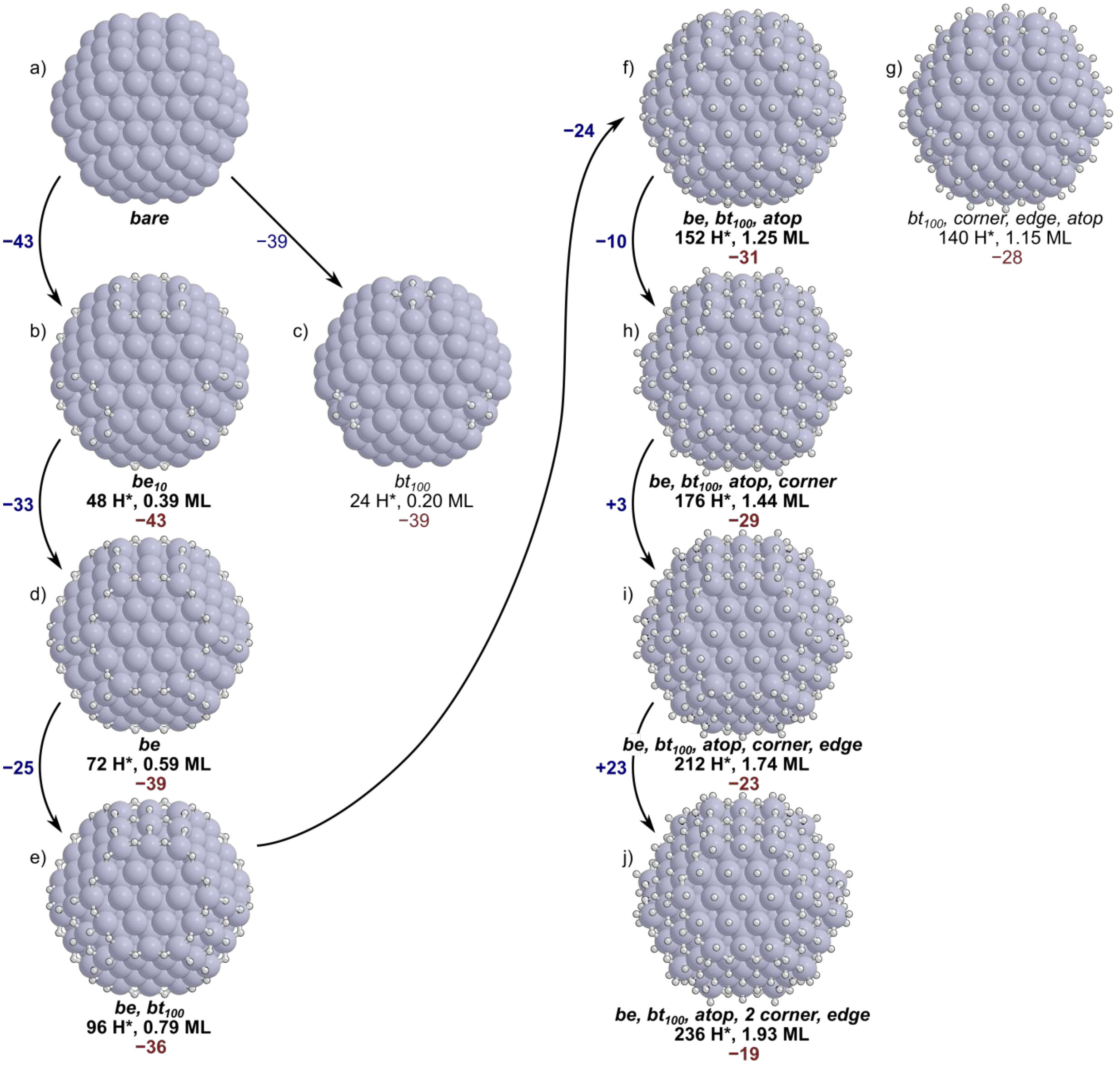

Figure S8. Adsorption of H* onto Pt_{201} clusters (with 122 Pt_s atoms) in adlayers that predominantly feature atop-bound H* atoms on (111) terrace regions and bridge-bound H* atoms on (100) terraces and on corner and edge atoms surrounding terraces. The binding modes occupied by H* are labeled along with the total number of H* atoms and the H* coverage beneath each particle. Average H* adsorption energies (corresponding to ½ n $H_2(g) + n^* \rightarrow n$H*; $\Delta H_{H*,ads}$, Eq. SI-41) are shown beneath each particle in red, and average differential H* adsorption energies (corresponding to ½ x $H_2(g) + n H^* + x^* \rightarrow (n+x)H^*$; $\delta H_{H*,ads}$, Eq. SI-42) are shown in blue along arrows depicting adsorption events.

SI-8 Derivation of Rate Equations for DFT-derived H_2-D_2 Exchange Mechanism

$$H_2 + 2^* \underset{k'_{-1}}{\overset{k'_1}{\rightleftarrows}} 2H^* \qquad \text{[S4.1]}$$

$$HD + 2^* \xleftarrow[k'_{-2}]{} H^* + D^* \qquad \text{[S4.2]}$$

$$D_2 + 2^* \underset{k'_{-3}}{\overset{k'_3}{\rightleftarrows}} 2D^* \qquad \text{[S4.3]}$$

$$H_2 + H^* + {}' \underset{k'_{-4}}{\overset{k'_4}{\rightleftarrows}} H' + H^* + H' \qquad \text{[S4.4]}$$

$$H_2 + D^* + {}' \underset{k'_{-5}}{\overset{k'_5}{\rightleftarrows}} D' + H^* + H' \qquad \text{[S4.5]}$$

$$HD + H^* + {}' \xleftarrow[k'_{-6}]{} H' + H^* + D' \qquad \text{[S4.6]}$$

$$HD + H^* + {}' \xleftarrow[k'_{-7}]{} H' + D^* + H' \qquad \text{[S4.7]}$$

$$HD + D^* + {}' \xleftarrow[k'_{-8}]{} D' + H^* + D' \qquad \text{[S4.8]}$$

$$HD + D^* + {}' \xleftarrow[k'_{-9}]{} D' + D^* + H' \qquad \text{[S4.9]}$$

$$D_2 + H^* + {}' \underset{k'_{-10}}{\overset{k'_{10}}{\rightleftarrows}} H' + D^* + D' \qquad \text{[S4.10]}$$

$$D_2 + D^* + {}' \underset{k'_{-11}}{\overset{k'_{11}}{\rightleftarrows}} D' + D^* + D' \qquad \text{[S4.11]}$$

Scheme S4. Proposed DFT-derived intermediate steps for H_2-D_2 reactions on Pt surfaces. DFT methods use only H_2-H_2 reactions.[†]

Scheme S4 assumes that any kinetic isotope effects depend only on the isotopic content of the reaction. The rate for HD formation ($r_{HD,f}$) from the elementary steps in Scheme S4 is given by:

[†] This scheme is identical to Scheme 2 in the main text.

$$r_{HD,f} = k'_{-2}\theta_H\theta_D + k'_{-6}\theta'_H\theta_H\theta'_D + k'_{-7}\theta'_H\theta_D\theta'_H + k'_{-8}\theta'_D\theta_H\theta'_D + k'_{-9}\theta'_D\theta_D\theta'_H \qquad (SI-43)$$

Here, θ_H and θ_D are the fractional coverage of atop sites by H and D adatoms, respectively, and θ'_H and θ'_D are the fractional coverage of fcc sites. We apply the pseudo-steady-state approximation (PSSA) to H*

$$\begin{gathered} 2r_{4.1} + r_{4.5} + r_{-4.7} + r_{-4.10} = \\ 2r_{-4.1} + r_{-4.2} + r_{-4.5} + r_{-4.8} + r_{4.10} \end{gathered} \qquad (SI-44)$$

$$\begin{gathered} 2k'_1(H_2)(*)^2 + k'_5(H_2)(D*)(') + k'_{-7}(H')(D*)(H') + k'_{-10}(H')(D*)(D') = \\ k'_{-1}(H*)^2 + k'_{-2}(H*)(D*) + k'_{-5}(D')(H*)(H') + k'_{-8}(D')(H*)(D') + k'_{10}(D \end{gathered} \qquad (SI-45)$$

D*

$$\begin{gathered} 2r_{4.3} + r_{-4.5} + r_{-4.8} + r_{4.10} = \\ r_{-4.2} + 2r_{-4.3} + r_{4.5} + r_{-4.7} + r_{-4.10} \end{gathered} \qquad (SI-46)$$

$$\begin{gathered} 2k'_3(D_2)(*)^2 + k'_{-5}(D')(H*)(H') + k'_{-8}(D')(H*)(D') + k'_{10}(D_2)(H*)(') = \\ k'_{-2}(H*)(D*) + k_{-3}(D*)^2 + k'_5(H_2)(D*)(') \;\; + k'_{-7}(H')(D*)(H') + k'_{-10}(H \end{gathered} \qquad (SI-47)$$

H’

$$\begin{gathered} 2r_{4.4} + r_{4.5} + r_{4.10} = \\ 2r_{-4.4} + r_{-4.5} + r_{-4.6} + 2r_{-4.7} + r_{-4.9} + r_{-4.10} \end{gathered} \qquad (SI-48)$$

$$\begin{gathered} 2k'_4(H_2)(H*)(') + k'_5(H_2)(D*)(') + k'_{10}(D_2)(H*)(') = \\ 2k'_{-4}(H')(H*)(H') + k'_{-5}(D')(H*)(H') + k'_{-6}(H')(H*)(D') \\ +2k'_{-7}(H')(D*)(H') + k'_{-9}(D')(D*)(H') + k'_{-10}(H')(D*)(D') \end{gathered} \qquad (SI-49)$$

and D’

$$\begin{gathered} r_{4.5} + r_{4.10} + 2r_{4.11} = \\ r_{-4.5} + r_{-4.6} + 2r_{-4.8} + r_{-4.9} + r_{-4.10} + 2r_{-4.11} \end{gathered} \qquad (SI-50)$$

$$\begin{gathered} k'_5(H_2)(D*)(') + k'_{10}(D_2)(H*)(') + 2k'_{11}(D_2)(D*)(') = \\ k'_{-5}(D')(H*)(H') + k'_{-6}(H')(H*)(D') + 2k'_{-8}(D')(H*)(D') \\ + k'_{-9}(D')(D*)(H') + k'_{-10}(H')(D*)(D') + 2k'_{-11}(D')(D*)(D') \end{gathered} \qquad (SI-51)$$

The surface is assumed to be fully saturated (at atop sites) during all H_2-D_2 exchange experiments, such that:

$$\theta_H + \theta_D = 1 \qquad (SI-52)$$

The fcc sites are assumed to be nearly bare; the fraction of free fcc sites (θ'_s) is therefore assumed to be unity:

$$\theta'_s = 1 \qquad (SI-53)$$

Equations SI-42 – SI-51 can be solved simultaneously to give fractional coverages of H*, D*, H’ and D’. In the absence of any KIE ($k_1 = k_3$; $k_{-1} = k_{-2} = k_{-3}$; $k_4 = k_5 = k_6 = k_7$; $k_{-4} = k_{-5} = k_{-6} = k_{-7}$), these are given by:

$$\theta_H = \frac{(H_2)}{(H_2) + (D_2)} \qquad (SI-54)$$

$$\theta_D = \frac{(D_2)}{(H_2) + (D_2)} \qquad (SI-55)$$

$$\theta'_H = \frac{\sqrt{k_4}(H_2)}{\sqrt{k_{-4}}\sqrt{(H_2) + (D_2)}} \qquad (SI-56)$$

$$\theta'_D = \frac{\sqrt{k_4}(D_2)}{\sqrt{k_{-4}}\sqrt{(H_2) + (D_2)}} \qquad (SI-57)$$

The equation for the formation rate of HD (Eq. SI-43) can therefore be written as:

$$r_{HD,f} = k'_{-2}\frac{(H_2)(D_2)}{((H_2) + (D_2))^2} + 2k_4\frac{(H_2)(D_2)}{(H_2) + (D_2)} \qquad (SI-58)$$

SI-9 DFT-derived Transition States and Enthalpy Barriers for H_2-H* Reactions in H*(fcc)-dominated Adlayers on Pt(111) Surfaces and Pt_{201} Particles

H_2-Pt interactions and the dissociation of H_2 molecules may be facilitated by displacing H adatoms to alternate binding sites (Section 3.6). Such mechanisms may occur on H*-covered surfaces with H* bound primarily at atop sites, where the atop-bound H adatoms are displaced to fcc sites, or with H* bound primarily at fcc surfaces, where fcc-bound H adatoms are displaced to atop sites. The binding enthalpy of H at each of these sites is similar and within the inaccuracies of theoretical calculations. Activation barriers were therefore investigated for H* in both configurations. Activation barriers in H*(atop)-adlayers on Pt(111) surfaces and Pt_{201} surfaces were presented in Section 3.6 and are shown here for H*(fcc)-adlayers here. Figure S10 shows DFT-derived transition state structures H_2 activation routes on Pt(111) surfaces at 1 H*/Pt_s. Figure S11 shows DFT-calculated H_2 activation transition states on Pt_{201} particles for H* coverages of 1.38–1.67 H*/Pt_s. These activation barriers were higher than those obtained on equivalent atop configurations; activation barriers on atop-dominated adlayers therefore gave better agreement with the experimental data (Table 2; Section 3.5).

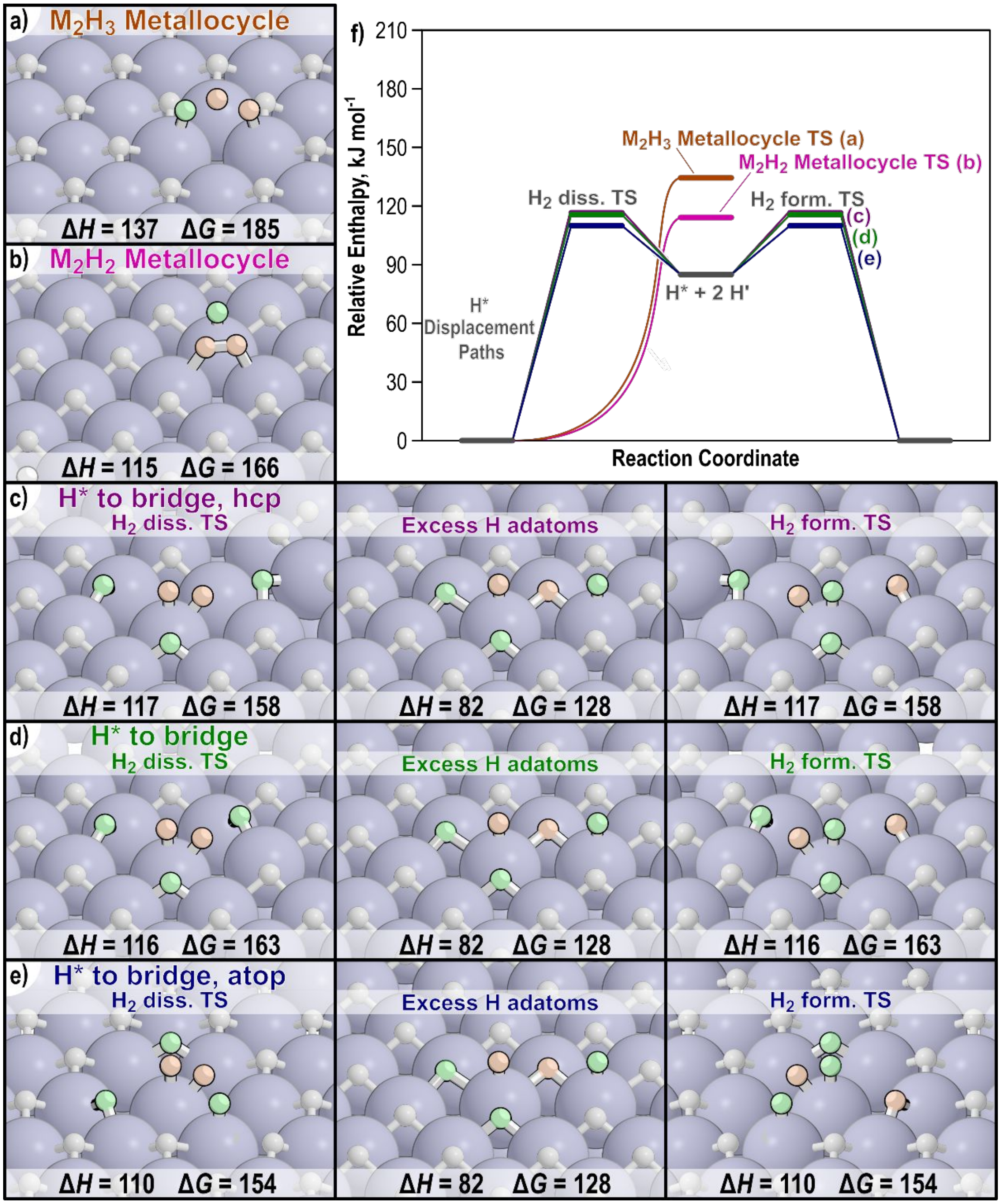

Figure S10. DFT-derived transition state structures for five H_2 activation routes on Pt(111) surfaces at 1 H*/Pt_s coverages with H* in fcc positions. DFT-derived enthalpies (Δ*H*) and free energies (Δ*G*) are shown (at 383 K, 1 bar) relative to a H*-covered surface and H_2(g) for each structure and in the inset reaction coordinate diagram. Reaction mechanisms include those mediated by transition states involving **a)** a M_2H_3 metallocycle (orange), **b)** a M_2H_2 metallocycle (pink), or the displacement of H* to a **c)** vicinal bridge and hcp sites (purple), **d)** vicinal bridge sites (green), and **e)** vicinal bridge and atop sites (blue). Atoms highlighted in orange reflect those from gas-phase H_2, those highlighted in green reflect H* atoms that are reacting directly with H_2 in parts a and b or displaced to adjacent binding modes to accommodate the H_2 dissociation transition state for routes c-e.

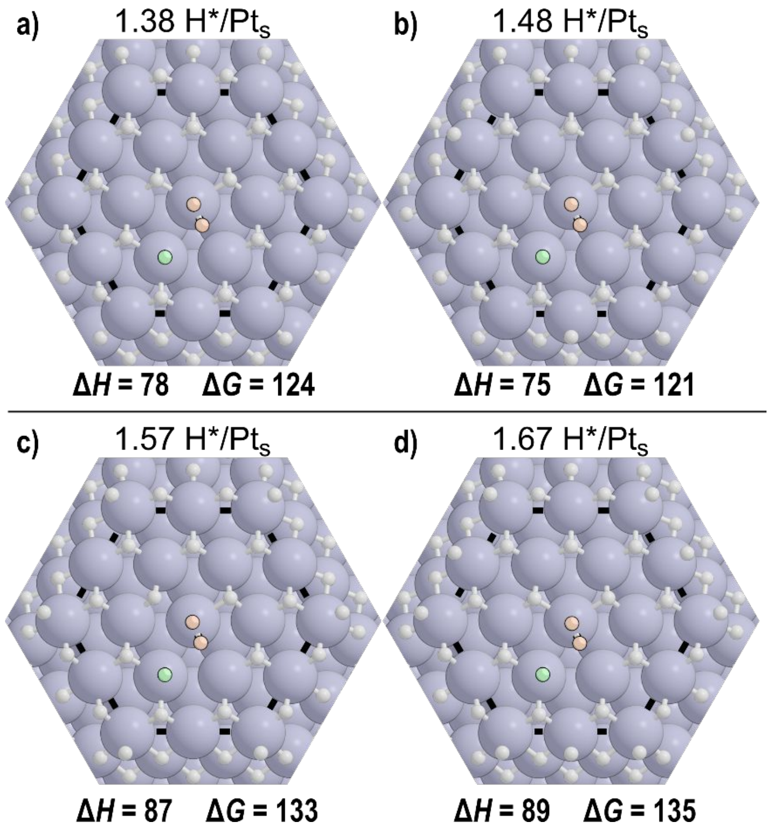

Figure S11. DFT-calculated H_2 activation transition states on Pt_{201} particles with H* in fcc binding modes on the (111) terraces at H* coverages of 1.38–1.67 H*/Pt_s. The H_2 (atoms highlighted in orange) activation mechanism involves displacing H* from an fcc site to an atop fcc site (atoms highlighted in green). Activation enthalpies and free energies (383 K, 1 bar) are shown relative to H*-covered particle surfaces and gas-phase H_2.